Large-scale timing synchronization based on linear-optics timing detectors

Tong Wang[1], Mingzhe Li[1], Yi Zhang[1], Jie Yang[1], Yulin Shen[1], Ke Zhang[1], Dehui Pan[1], Jiahui Yao[1], Haoyang Sun[1] and Ming Xin[1,2,*]

[1] *School of Electrical and Information Engineering, Tianjin University, Tianjin, 300072, China,*
[2] *Tianjin Key Laboratory of Brain-Inspired Intelligence Technology, Tianjin, 300072, China*

Correspondence to: School of Electrical and Information Engineering, Tianjin University. Email: xinm@tju.edu.cn

Abstract We presented an attosecond-precision timing detector based on linear-optics. The minimum measurement floor is 1×10^{-10} fs^2/Hz with only 1-mW input optical power. With this novel technique, the residual dispersion of 5.2-km fiber link is characterized and precisely compensated. Finally, a comprehensive feedback model has been developed to analyze the noise coupling in a long-distance link stabilization system. The simulation results demonstrate an out-of-loop jitter of merely 359 as, integrated at [1 Hz, 1 MHz], at 1-mW input power per photodetector of our timing detector. Remarkably, the system is capable of maintaining sub-femtosecond precision even at optical power levels as low as 240 nW (for 5.2-km link length), or the link length as long as 20 km (with 1 μW optical power), respectively.

This peer-reviewed article has been accepted for publication but not yet copyedited or typeset, and so may be subject to change during the production process. The article is considered published and may be cited using its DOI.

10.1017/hpl.2025.30

Key words: *timing synchronization, dispersion compensation, link stabilization, metrology.*

I. INTRODUCTION

Precise timing synchronization is tremendous in the large-scale scientific facilities [1]. For instance, in high-power laser facilities (HPLF) such as SG-II project [2] in China, HERCULES laser [3, 4], SULF laser [5], the J-KAREN-P laser [6] and the Texas Petawatt Laser [7], coherent beam combining (CBC) is regarded as a promising approach to increase the extreme intensity [8-10]. The key to achieving high-efficiency CBC lies in ensuring that each individual laser is precisely spatially co-aligned and timing-synchronized with exceptional precision. To achieve even greater laser intensities, ultrahigh-power laser facilities including Apollon [11], ELI-NP [12], EP-OPAL [13], and SEL [14], capable of delivering outputs of 10 PW and above are currently being developed, in which timing synchronization plays an even more important role. In addition to HPLF, the next generation X-ray free electron lasers (XFELs) have also garnered significant global attention [15], such as the European XFEL in Hamburg, FERMI [16] in Italy, SwissFEL in Switzerland, and the Linac Coherent Light Source (LCLS) [17] along with LCLS II at Stanford [18]. To achieve the goal of generating attosecond (as, 10^{-18}s) X-ray pulses [19] of unparalleled brightness and filming ultrafast physical and chemical processes with spatial- temporal resolution of atoms, the attosecond-precision timing synchronization is exigently required.

A typical synchronization system comprises a timing reference that produces exceptionally stable timing signals, a target signal that requires alignment, a timing detector that assesses the timing difference between the target and reference signals, and a control unit that adjusts the timing of the target to match the reference. When the target device is located far from the reference, a timing link is essential to convey the timing signal from the reference to the target [20].

https://doi.org/10.1017/hpl.2025.30 Published online by Cambridge University Press

Passive mode-locked laser (MLL), which shows ultralow timing jitter at high frequencies (e.g., < 1 fs above 10 kHz) [21] is considered as an ideal timing reference for synchronizing multiple microwave and optical sources. To break the limitation of AM-PM noise and provide high timing resolution for the synchronization system, the balanced optical cross-correlator (BOC) [22, 23] scheme was introduced. Over the past decades, the pulse-based BOC timing synchronization method has benefited several extreme laser facilities such as SULF, ELI, European XFEL, FERMI, SwissFEL and LCLS II.

However, as the whole science facilities become steadily complex, the limitations of BOC timing synchronization system are gradually emerging. Currently, the primary challenge facing BOC-based timing synchronization systems lies in the inherent contradiction between optical power and synchronization precision. To ensure sub-fs synchronization precision while simultaneously suppressing additional timing jitter induced by fiber nonlinear effects [20], the optical power transmitted through the link must be constrained within the range of 10 to 20 mW. Taking transmission losses into account, this constraint limits the link length to under 5 kilometers. And since the output power of an MLL oscillator is usually 100~200 mW, the maximum number of synchronization terminals is also limited to ~10. Such limitations significantly impede the scalability of femtosecond-pulse-based timing synchronization technology towards greater distances and larger-scale implementations, thereby failing to meet the growing demands of large scientific facilities in terms of both physical dimensions and the number of terminal nodes.

To improve the scalability of these large facilities and ensure their continued operation with remarkable stability over the forthcoming decades, an ultra-precise timing and synchronization system which efficiently utilize optical power and maintain a compact layout is urgently desired. In this article, we have proposed a novel timing synchronization technology based on linear-optics

https://doi.org/10.1017/hpl.2025.30 Published online by Cambridge University Press

timing detectors [24]. Each timing link can be stabilized to sub-fs precision with <1 mW optical power, therefore, the additional timing jitter induced by fiber nonlinear effects can be neglected. This work would potentially extend synchronization distances from several kilometers to tens of kilometers, and enable a single MLL oscillator to synchronize hundreds of terminals rather than just a few, paving the way for more sophisticated and powerful scientific facilities.

In the following of this paper, the detailed theoretical and experimental demonstration of the linear-optics timing detector (LOTD) is first given in Section II and III. Using this timing detector, the residual dispersion of a 5.2-km fiber link is precisely compensated in Section IV. A detailed feedback model is then built to analyze the factors influencing the out-of-loop timing jitter in Section V. Finally, a simulation of the complete timing link stabilization system with our new timing method is presented, which can satisfy the critical and demanding synchronization needs of next-generation photon science facilities and will be experimentally carried out in our future work.

II. WORKING PRINCIPLE OF LOTD

Fig. 1(a) illustrates the basic principle of the LOTD. The input from the light laser source is injected into an acousto-optic modulator (AOM), which diffracts the pulse trains into different directions. A radio-frequency (RF) signal is then applied to the AOM to generate the original 0^{th} order light and the modulated 1^{st} order light. The timing target under measurement is placed in the path of the 1^{st} order light, introducing a perturbative timing error Δt to the optical signal. A 3-dB fiber coupler integrates the two diffracted light paths, generating beat note signals that are subsequently detected by a photodiode (PD).

For the input optical pulse train, we can describe its electric field by the following expression

$$E_0(t) = \sum_{k=-\infty}^{+\infty} A(t - kT)e^{-j\omega_0 t} \tag{1}$$

https://doi.org/10.1017/hpl.2025.30 Published online by Cambridge University Press

In Eq. (1), $A(t)$ characterizes the temporal envelope function, ω_0 defines the optical carrier frequency, and T represents the temporal separation between pulses. The optical fields entering the collimators from the 0th and 1st order diffraction light can be expressed as

$$E_0(t) = \sum_{k=-\infty}^{+\infty} A(t-kT)e^{-j\omega_0 t} = \sum_{n=-\infty}^{+\infty} A_n e^{-jn\omega_{rep}t} e^{-j\omega_0 t} \tag{2}$$

$$E_1(t) = \sum_{k=-\infty}^{+\infty} A(t-\Delta t-kT)e^{-j(\omega_0+\omega_{RF})(t-\Delta t)} = \sum_{n=-\infty}^{+\infty} B_n e^{-jn\omega_{rep}t} e^{-j(\omega_0+\omega_{RF})(t-\Delta t)} \tag{3}$$

where $f_{rep}=1/T$ is the pulse train's repetition frequency, f_{RF} is the frequency of the RF driving signal, $\omega_{rep}=2\pi f_{rep}$, $\omega_{RF}=2\pi f_{RF}$ and A_n, B_n are the Fourier series of the 0th and 1st order pulse train profiles. After passing through the coupler, the optical power reaching the PD is given by

$$P(t,\Delta t) \propto |E_0 - jE_1|^2 = |E_0|^2 + |E_1|^2 + j(E_0E_1^* - E_0^*E_1) \tag{4}$$

To filter out the ω_{RF} frequency component $P(t, \Delta t)$, we use a band pass filter (BPF). Thus, the output signal is given by

$$V_{BPF} \propto j\sum_{n=-\infty}^{+\infty}\left[A_nB_n^*e^{j[\omega_{RF}t-(\omega_0+\omega_{RF})\Delta t]} - A_n^*B_ne^{-j[\omega_{RF}t-(\omega_0+\omega_{RF})\Delta t]}\right] = X\cos\left[\theta+\omega_{RF}t-(\omega_0+\omega_{RF})\Delta t\right] \tag{5}$$

where $X=\left|\sum_{n=-\infty}^{+\infty}A_nB_n^*\right|$, $j\sum_{n=-\infty}^{+\infty}A_nB_n^* = Xe^{j\theta}$. It should be noted that the timing information Δt is reflected in both the amplitude and phase part of V_{BPF}. To eliminate the distraction of the phase component, a zero-bias Schottky diode (ZSD) is employed to extract the power fluctuation of V_{BPF}, thereby simplifying the resolution of Δt. Using the principle of Parseval's theorem, the ZSD response can be formulated as

$$V_{ZSD}(\Delta t) \propto \left|\sum_{n=-\infty}^{+\infty}A_nB_n^*\right|^{\alpha} \propto \left|\int_{-\infty}^{+\infty}A(t)A(t-\Delta t)dt\right|^{\alpha} \tag{6}$$

where α denotes a parameter linked to the nonlinear behavior of the ZSD. Hence, the timing characterization curve that indicates the relationship between timing error Δt and V_{ZSD} can be derived. Suppose $A(t)$ is a hyperbolic secant function [25]:

https://doi.org/10.1017/hpl.2025.30 Published online by Cambridge University Press

$$A(t) = A_0 \,\mathrm{sech}(t/\tau) \tag{7}$$

where τ is a parameter that characterizes the pulse width. Substituting (7) into (6), the analytical solution of V_{ZSD} can be further derived as:

$$V(\Delta t) \propto \begin{cases} \left[\dfrac{4\Delta t e^{\Delta t/\tau}}{e^{2\Delta t/\tau}-1}\right]^{\alpha}, & \Delta t \neq 0 \\ (2\tau)^{\alpha}, & \Delta t = 0 \end{cases} \tag{8}$$

To eliminate all the trivial coefficients, the normalized voltage can be used:

$$V_{norm}(\Delta t) = \frac{V(\Delta t)}{V(0)} = \left[\frac{2\dfrac{\Delta t}{\tau}e^{\Delta t/\tau}}{e^{2\Delta t/\tau}-1}\right]^{\alpha} \tag{9}$$

A simulated normalized timing curve is given in Fig. 1(b). On either side of this curve, V_{norm} shows a consistent and monotonic change with Δt, which means it can used to characterize Δt. In the magnified portion, the maximum slope of 0.0018 fs^{-1} is obtained, giving the maximum timing sensitivity. Based on Eq. (9), the normalized timing sensitivity is given by

$$\frac{dV_{norm}}{d\Delta t} = \frac{1}{\tau} f(x) \tag{10}$$

where

$$x = \frac{\Delta t}{\tau} \tag{11}$$

https://doi.org/10.1017/hpl.2025.30 Published online by Cambridge University Press

$$f(x)=2\alpha\left[\frac{2xe^{x}}{e^{2x}-1}\right]^{\alpha-1}e^{x}\frac{e^{2x}(1-x)-(1+x)}{(e^{2x}-1)^{2}} \tag{12}$$

Fig. 1(c) shows the relationship between the normalized timing sensitivity and Δt. At the two peaks, the maximum sensitivity can be achieved when $\Delta t=\pm 1.6061\tau$.

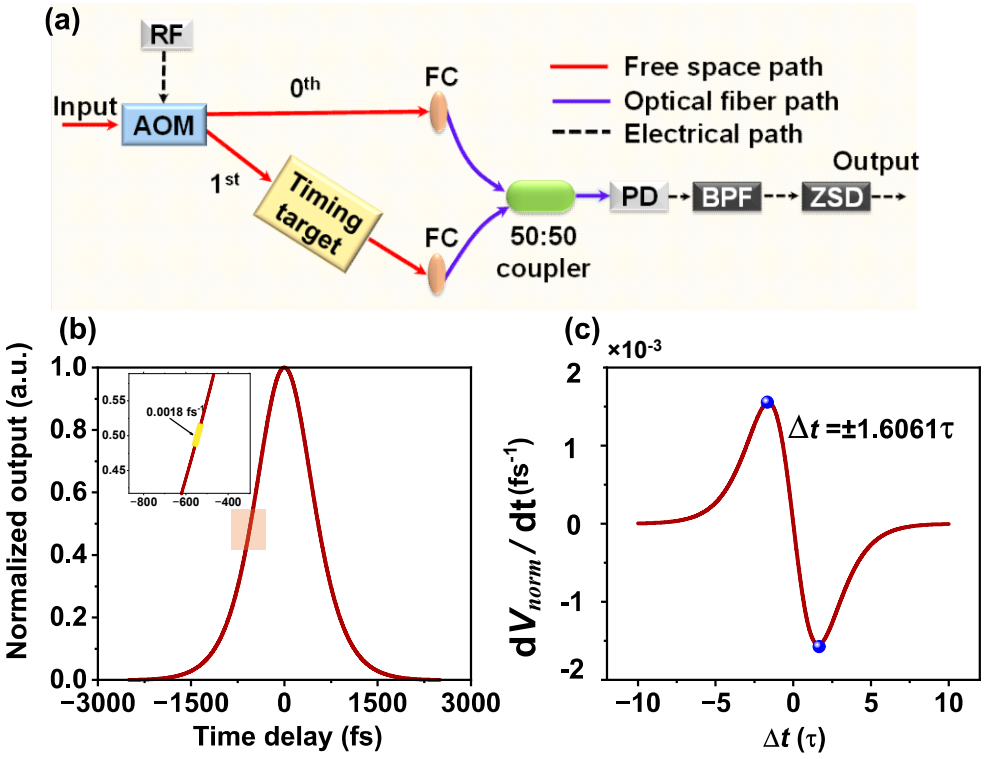

Fig.1 (a)Basic concept of the LOTD. FC, fiber collimator. (b)Simulated timing characterization curve, α=1, τ=170 fs. (c)Normalized timing sensitivity with different timing error.

The balanced detection is commonly employed to effectively lower the timing detection floor. A typical balanced operation consists of two identical timing detection circuits with a relative time delay, as shown in Fig.2 (a). The 0th order light from the AOM is split into two paths, one of which incorporates a fixed delay T_D. Simultaneously, the 1st order diffraction light is divided via a 50:50 coupler: one branch combines with the undelayed 0th order light, while the other combines with the T_D-delayed 0th order light through two additional 50:50 couplers.

https://doi.org/10.1017/hpl.2025.30 Published online by Cambridge University Press

Both combined beams are processed through PD, BPF and ZSD to generate independent timing signals. By differentially analyzing these two outputs, common-mode noise such as laser amplitude fluctuations and environmental disturbances are theoretically canceled, thereby enhancing the timing precision.

The balanced output voltage is given by

$$V_B(\Delta t) = V_{norm}(\Delta t - T_D) - V_{norm}(\Delta t) \tag{13}$$

and the corresponding timing curve becomes an "s" shape, as depicted in Fig. 2(b). At the zero-crossing Δt_0 of this curve, $V_B(\Delta t_0) = 0$, i.e., $V_{norm}(\Delta t_0 - T_D) = V_{norm}(\Delta t_0)$. Based on the symmetry of $V_{norm}(\Delta t)$, $\Delta t_0 = T_D/2$. In order to attain maximum timing sensitivity at the crossing point, the slope of $V_{norm}(\Delta t - T_D)$ and $V_{norm}(\Delta t)$ at $\Delta t = \Delta t_0$ need to be maximum and minimum, respectively. Therefore, the optimum delay time for balanced detection is $T_D = \pm 3.2122\ \tau$ (The detailed relation between $dV_B/d\Delta t$ and T_D are given in Fig. 2(c)). In Fig. 2(b), several balanced timing curves with different T_D values are plotted, the one with T_D=550 fs (closest to 3.2122 τ) gives the maximum timing sensitivity around the zero-crossing point.

The LOTD has two key inherent advantages that make it well-suited for various applications. First, if the 0th and 1st order pulse trains have the same chirp, the dispersion phase coefficients can be canceled by the product A_nB_n* in Eq. (6). Therefore, transform-limited pulse widths are not essential for maintaining high timing detection sensitivity. This characteristic is particularly beneficial in situations where it is difficult or cost-prohibitive to compensate for high-order dispersion, yet identical chirp between two pulse trains is readily achievable, as exemplified in ultra-long fiber loop-based timing sensors. Additionally, it offers enhanced timing resolution at low power levels when compared to nonlinear-optics-based detectors like BOC. Taking advantage

https://doi.org/10.1017/hpl.2025.30 Published online by Cambridge University Press

of this merit, it is possible to perform timing link stabilization with ultra-low optical power, which will be discussed in Section V.

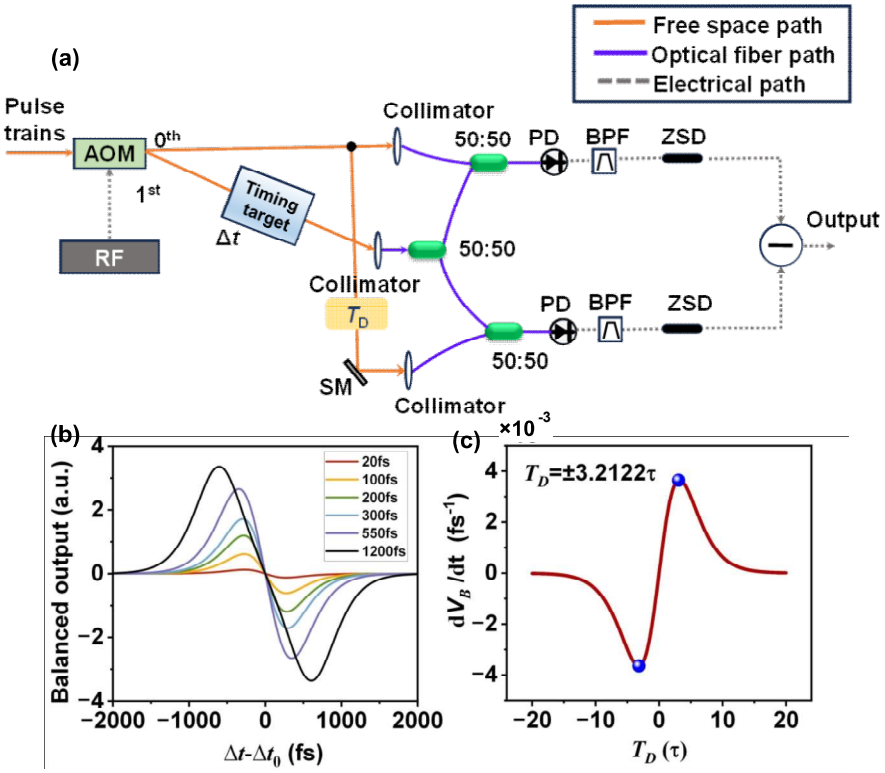

Fig.2 (a)Basic concept of the LOTD using balanced structure. (b)Balanced timing characterization curve with different delay T_D. (c)Balanced normalized timing sensitivity with different delay T_D.

III. BLOTD Experimental Characteristics

The detailed experimental setup of the balanced linear-optics timing detector (BLOTD) is presented in Fig. 3(a). A stable mode-locked laser source (MENHIR-1550) generates pulse trains centered at 1555 nm with 216.667-MHz repetition frequency and 170-fs duration, and subsequently injected into an AOM. An 80-MHz sinusoidal waveform from a function generator, initially at 200 mV RMS, is amplified to 36 dBm to drive the AOM. The power distribution between the 0^{th} and 1^{st} order paths of diffraction light should be near-equal.

A motorized delay line (MDL) is positioned in the 1^{st} order path to introduce a time delay Δt between the two beams. **Balanced detection requires two independent timing measurement**

https://doi.org/10.1017/hpl.2025.30 Published online by Cambridge University Press

circuits for the 0th- and 1st- order light. In the first circuit, the relative time delay between the two beams is Δt, while the second circuit introduces an additional delay T_D (total: $\Delta t+T_D$). To implement this, the 0th-order light from the AOM is split into two paths via a PBS. The light in one path is reflected by a silver mirror (SM) mounted on a manual stage, so as to pass twice through a quarter-wave plate. By finely adjusting the distance between the SM and the PBS using the manual stage, the relative delay T_D for the optimal timing sensitivity near the zero-crossing point of the "s"-shaped curve can be obtained. With the help of three 50:50 fiber couplers, the 0th and 1st order pulse trains beat on two avalanche photodiode detectors (APD), and then two 80-MHz beat note signals can be obtained. The 100-MHz 3-dB bandwidth APD is customized with low NEP (2 pW/√Hz) and high responsivity (0.9-A/W). The beat note from each APD is initially extracted using a BPF and subsequently amplified by a low-noise amplifier (LNA). This process ensures that the power fluctuations, which contain the timing information of the beat note, are adequately amplified for further extraction by the ZSD. The balanced detection is finally achieved by differentially amplifying the two ZSDs' outputs. The differential amplifier is driven by a matched low-noise power supply. The timing characterization curve, which illustrates the relationship between Δt and the ZSD output, is generated by recording the output voltage through a data acquisition card (DAQ) while concurrently moving the computer-controlled MDL. With 1-mW power for each pulse train at each APD, the timing sensitivity around the zero-crossing is about 43.537 mV/fs, as shown in Fig. 3(b). Due to the nonuniformity of the two ZSDs, the s-like curve in Fig. 3(b) is a little asymmetric.

The timing jitter spectral density (TJSD) of the BLOTD is assessed by routing the output from the differential amplifier to the baseband port of a signal source analyzer (SSA). The findings are illustrated as the dark blue curve in Fig. 3(c). The lowest measured timing detection noise floor

https://doi.org/10.1017/hpl.2025.30 Published online by Cambridge University Press

reaches approximately 1×10^{-10} fs²/Hz, which is nearly at the shot noise limit (marked by the red dashed line). By opting for photodetectors with enhanced responsivity, it is feasible to further decrease the detection floor and approach the standard quantum limit for timing jitter in pulse trains, as predicted in reference [26] (represented by the blue dashed line), which is only 10 dB higher than the current detection threshold. Displayed at the bottom of Fig. 3(c) is the integrated timing jitter. The total integrated timing jitter (IDTJ) within the range of 1 Hz to 1 MHz is found to be only 26.57 as.

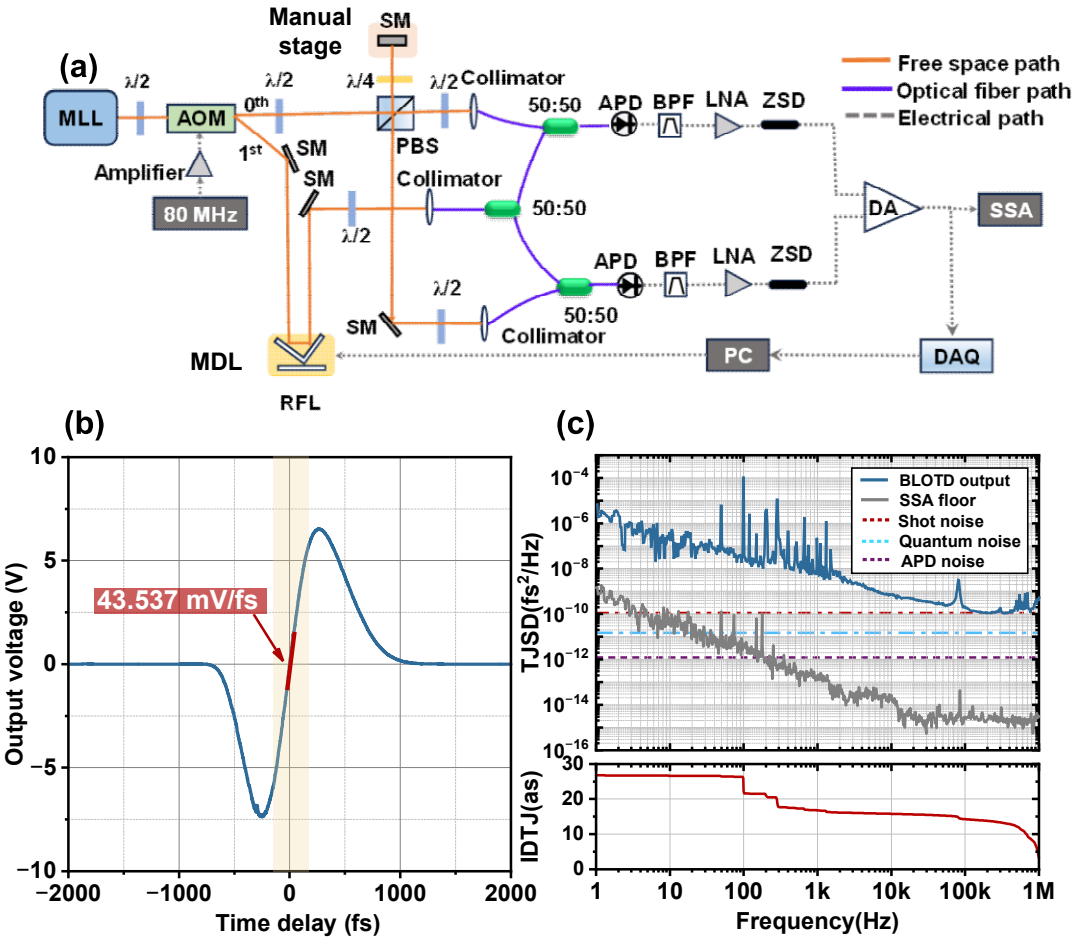

Fig. 3. (a)The experimental setup for the BLOTD. λ/2, half wave plate; λ/4, quarter wave plate; PBS, polarization beam splitter; RFL, retroreflector; 50:50, 3-dB coupler; PC, personal computer; DA, differential amplifier. (b)Measured balanced timing characterization curve. (c)Measured results: TJSD and corresponding IDTJ.

IV Residual Dispersion Compensation with LOTD

https://doi.org/10.1017/hpl.2025.30 Published online by Cambridge University Press

In a typical pulse-based large-scale timing synchronization system [20], the timing link is stabilized by comparing the relative timing error between the round-trip link pulse and the new incoming pulse from the master laser. The dispersion of the timing link needs to be carefully compensated to guarantee high precision timing detection as well as to restrict the Gordon-Haus timing jitter [27] generated during link transmission. In this section, with the help of LOTD, the residual dispersion of a timing link can be easily measured, and then accurate dispersion compensation can be performed afterwards.

In Eq. (6), if the 0^{th} and 1^{st} order pulse trains do not have the same chirp, the dispersion phase coefficients can no longer be canceled by the product A_nB_n*, which will broaden the timing curve. Therefore, the width of the timing curve can be used to characterize the link residual dispersion. The experimental setup is implemented in Fig. 4(a). The output of the MLL is separated into two paths. An AOM is placed in one path to shift the optical pulses' carrier frequency before they enter the timing link. The relative timing errors between the link pulse and the original laser pulse are measured by the LOTD electronics (PD, BPF and ZSD), and the timing curve can be obtained by moving the MDL. The timing link is composed of 4.5-km single-mode fiber (SMF) and 0.7-km dispersion compensating fiber (DCF). The DCF can compensate both the second and third order dispersion of the SMF simultaneously. To allow room for fine adjustments, the DCF overcompensates for the dispersion of about 10 m SMF.

https://doi.org/10.1017/hpl.2025.30 Published online by Cambridge University Press

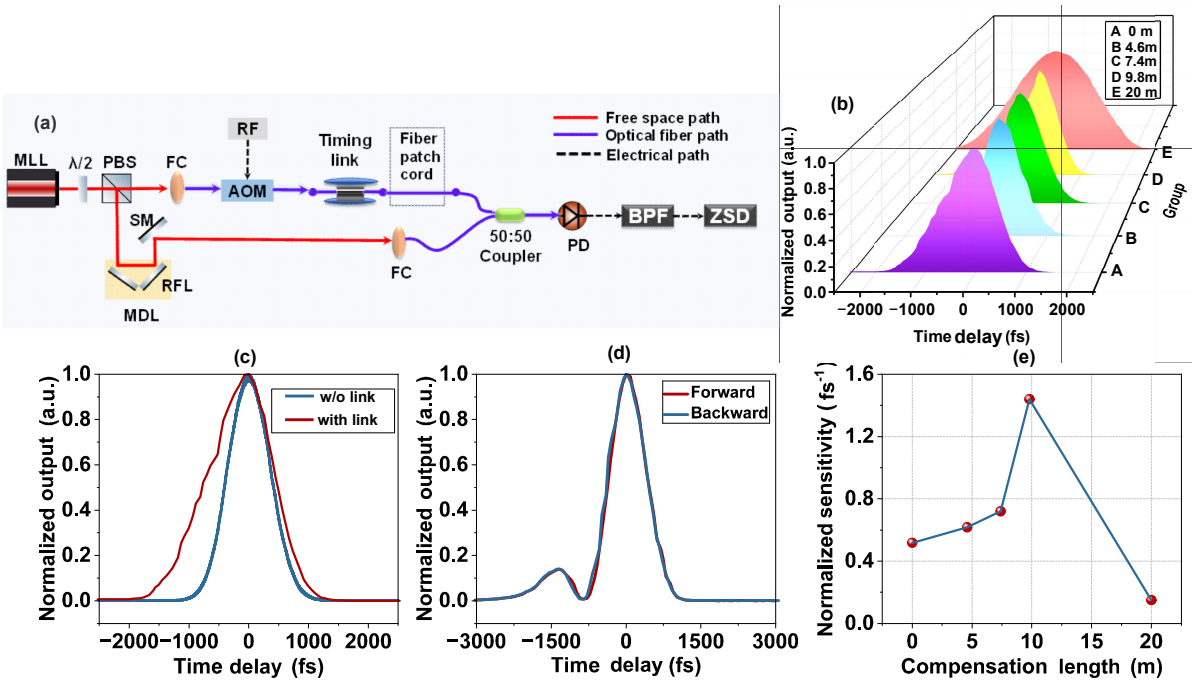

Fig.4 Experimental setup for residual dispersion compensation and results. (a) Experimental setups. (b)Timing curve with different fiber patch cord lengths. (c) Measured timing curves with and without the timing link. (d) Timing curve measured with MDL movements in the forward and backward directions. (e) Normalized timing sensitivity with different fiber patch cord lengths.

The measured timing curves with and without the timing link are compared in Fig. 4(c), obvious broadening effect is observed due to the links' residual dispersion. Different lengths of fiber patch cord are then introduced to fine tune the residual dispersion. With 4.8-m fiber patch cord, the two measured timing curves by moving the MDL in the forward and backward directions are compared in Fig. 4(d). The two curves exhibit near-perfect overlap, indicating that the temperature drift of the timing link does not affect the measurement results. The timing curves with different lengths of fiber patch cord are given in Fig. 4(b), and the maximum normalized timing sensitivity for each case is summarized in Fig. 4(e). With 9.8-m patch cord, the narrowest timing curve is obtained with the highest timing sensitivity, which means the residual dispersion of the timing link is almost compensated.

V Feedback model of the BLOTD-based timing link stabilization

https://doi.org/10.1017/hpl.2025.30 Published online by Cambridge University Press

After the timing link's dispersion is precisely compensated, it can be used to realize large scale remote timing synchronization. Fig. 5 gives a setup for timing link stabilization using BLOTD. In the link stabilization block, the input optical pulse train is divided into two pulse trains in the reference path and in the link path. The link path consists of a MDL, an AOM, a fiber stretcher, a dispersion-compensated fiber link, a 45° Faraday rotator and a 40/60 transmission/reflection fiber mirror. The 45° Faraday rotator can make sure that the polarization directions of forward and backward transmitted light in the link are orthogonal, so as to minimize the timing jitter induced by polarization mode dispersion. The relative timing error J_{IL} between the pulses in the reference and link path is measured by the in-loop BLOTD and fed back to control the fiber stretcher through a proportional integral (PI) controller, thus can stabilize the length of the timing link. In the out-of-loop measurement block, the residual timing jitter J_O between the link output pulse and the original pulse from the MLL is measured by the out-of-loop BLOTD, to evaluate the performance of the link stabilization.

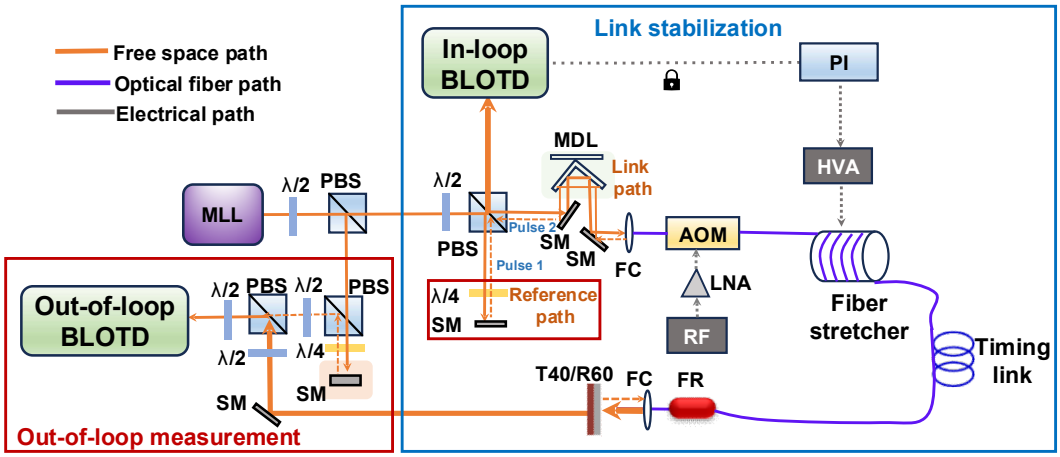

Fig. 5. Detailed scheme of the link network stabilization. HVA, high voltage amplifier; T40/R60, transmission 40%/ reflection 60% fiber mirror; FR, faraday rotator.

Since BLOTD is a linear-optics device, it is possible to operate this link stabilization with very low power levels. To investigate the minimum required optical power for sub-fs precision link stabilization, based on the setup in Fig. 5, a feedback model using experimental parameters is

https://doi.org/10.1017/hpl.2025.30 Published online by Cambridge University Press

constructed. The flow diagram of the feedback model is shown in Fig. 6.

The in-loop BLOTD detected timing jitter J_{IL} and the shot-noise-equivalent timing jitter J_S are converted to voltage signals with BLOTD transfer function H_{BLD}, amplified by the differential amplifier H_{DA} together with the electronic noise E_N (V/√Hz), and then sent to the PI controller H_{PI}. The output of the PI controller with additive noise E_{PI} then undergoes amplification and subsequent conversion to timing delays J_C through the fiber stretcher transfer function H_{FS}, J_C acts as a compensating jitter to maintain the lock. Due to the round-trip link propagation, J_C is added to the link delay twice, and the round-trip link propagation time $2T_L$ is accounted in for both J_C and the mode-locked laser's inherent jitter J_I. Whereas single-trip link propagation time T_L is utilized for environmental jitter J_E, as the latter integrates all the single-trip environmental jitter in its definition. For the out-of-loop measurement, J_C and J_I experience a single-pass link propagation delay T_L. All the noise sources J_I, J_E, J_S, E_N, E_{PI} are characterized with the method in Appendix A. The transfer functions can be calculated by the equations given in Appendix B.

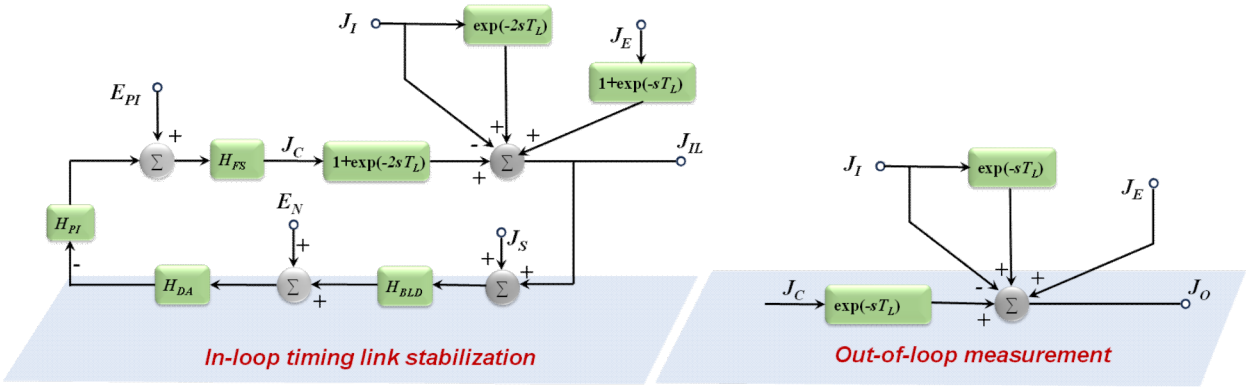

(a) (b)

Fig. 6. Feedback flow diagrams of (a) timing link stabilization (b) the out-of-loop jitter measurement. ω is the complex frequency, and $s=j\omega$; J_I, inherent jitter of the mode-locked laser; J_E, environmental jitter imposed on the link for single-trip link transmission; J_{IL}, detected timing jitter by the in-loop BLOTD; H_{BLD}, transfer function of the in-loop BLOTD; E_N, electronic noise in the in-loop BLOTD electronics; H_{DA}, transfer function of the differential amplifier in the BLOTD; H_{PI}, transfer function of the PI controller; E_{PI}, electronic noise of the PI controller; H_{FS} transfer function of the fiber stretcher; J_C, equivalent timing delay generated by the control loop

https://doi.org/10.1017/hpl.2025.30 Published online by Cambridge University Press

for compensation; J_S, shot-noise-equivalent timing jitter; T_L, single-trip link transmission time; J_O, relative timing jitter between the link output pulses and the original pulses from the mode-locked laser.

Based on Fig. 6, we have

$$J_{IL} = J_I[\exp(-2sT_L) - 1] + J_E[\exp(-sT_L) + 1] + J_C[\exp(-2sT_L) + 1] \tag{14}$$

$$J_C = \left[-\left(J_{IL} H_{BLD} + J_S H_{BLD} + E_N \right) H_{DA} H_{PI} + E_{PI} \right] H_{FS} \tag{15}$$

$$J_O = J_I \left[\exp(-sT_L) - 1 \right] + J_E + J_C \exp(-sT_L) \tag{16}$$

Substituting (14) and (15) into (16), the explicit expression of J_O can be derived as

$$J_O = C_I J_I + C_E J_E + C_S J_S + C_N E_N + C_{PI} E_{PI} \tag{17}$$

where

$$C_I = \left[\exp(-sT_L) - 1 \right] \frac{1 + H\left[1 - \exp(-sT_L)\right]}{1 + H\left[1 + \exp(-2sT_L)\right]} \tag{18}$$

$$C_E = \frac{1 + H\left[1 - \exp(-sT_L)\right]}{1 + H\left[1 + \exp(-2sT_L)\right]} \tag{19}$$

$$C_S = -\frac{H \exp(-sT_L)}{1 + H\left[1 + \exp(-2sT_L)\right]} \tag{20}$$

$$C_N = -\frac{H_{DA} H_{PI} H_{FS} \exp(-sT_L)}{1 + H\left[1 + \exp(-2sT_L)\right]} \tag{21}$$

$$C_{PI} = \frac{H_{FS} \exp(-sT_L)}{1 + H\left[1 + \exp(-2sT_L)\right]} \tag{22}$$

$$H = H_{BLD} H_{DA} H_{PI} H_{FS} \tag{23}$$

https://doi.org/10.1017/hpl.2025.30 Published online by Cambridge University Press

All the noise contributions C_iJ_i (i=E, S, I) and C_jE_j (j= N, PI) on the right side of Eq. (17) are mutually uncorrelated, the mean values of their cross products are cancelled. Consequently, the average out-of-loop jitter spectral density (s²/Hz) can be represented as:

$$J_O^2 = |C_I|^2 \overline{J_I^2} + |C_E|^2 \overline{J_E^2} + |C_S|^2 \overline{J_S^2} + |C_N|^2 \overline{E_N^2} + |C_{PI}|^2 \overline{E_{PI}^2} \tag{24}$$

As Eq. (24) indicates, J_O has five main contributions: the environmental noise imposed on the link, the electronic noise of the BLOTD, the noise introduced by the PI controller, the shot noise and the inherent jitter of the MLL, with coefficients C_E, C_N, C_{PI}, C_S and C_I, respectively. Fig. 7(a-e) present the calculated coefficients $|C_i|$ (i=E, N, PI, S, I) with 10.4-km link length for several distinct PI controller gain settings. To effectively reduce environmental noise and laser's inherent noise at frequencies lower than 5 kHz, it is essential to maintain high gain settings, as demonstrated in Fig. 7(a) and Fig. 7(e). Nevertheless, elevating the gain leads to increased BLOTD electronic noise and shot noise, as illustrated in Fig. 7(b) and Fig. 7(d). The large gain peaks can be observed near frequencies $n/4T_L$ (n=1, 3, 5…) as well as the fiber stretcher's resonant frequency (approximately 18 kHz) in Fig. 7(a)-(e).

https://doi.org/10.1017/hpl.2025.30 Published online by Cambridge University Press

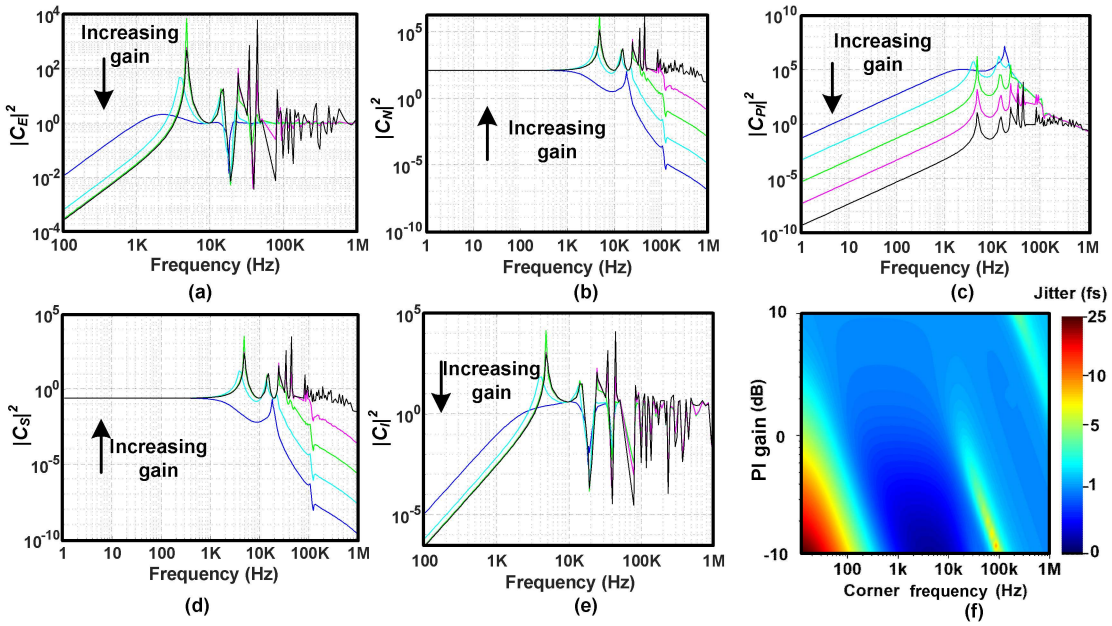

Fig. 7. Simulation results for a 10.4-km timing link stabilization system. (a) The coefficient for the environmental noise imposed on the link; (b) the coefficient for the electronic noise; (d) the coefficient for the noise from PI controller; (d) the coefficient for the shot noise; (e) the coefficient for the laser's inherent jitter; (f) out-of-loop integrated timing jitter with different PI gains and corner frequencies (1-mW optical power at each PD of the in-loop BLOTD).

Using the calculated coefficients above, each noise contributions in Eq. (24) as well as J_O^2 can be calculated. Typical experimental parameters are used in the simulation as given in Table.1 of Appendix C. Firstly, the optical power at each PD of the in-loop BLOTD is set as 1 mW. Through continuous optimization of the PI gain and corner frequency, we can achieve optimal link stabilization with minimal integrated timing jitter of J_O^2, as shown in Fig. 7(f). With the optimized PI controller settings, the TJSD of J_O^2 and each noise contributions are given in Fig. 8(a). The total IDTJ from 1 Hz to 1 MHz is only 0.36 fs (black curve). The environmental jitter of the link (pink curve) is the predominant noise factor in the low-frequency range. The inherent noise contribution of the MLL becomes more noticeable for offset frequencies above 100 Hz.

To investigate the link stabilization performance at ultra-low power levels, the optical power at each PD of the in-loop BLOTD is reduced to 1 μW. After re-optimizing the PI controller

https://doi.org/10.1017/hpl.2025.30 Published online by Cambridge University Press

parameters, the TJSD and IDTJ results are shown in Fig. 8(b), the timing link can still maintain sub-fs precision with 0.48 fs IDTJ at [1 Hz, 1MHz]. To compensate the low timing sensitivity of BLOTD at 1-μW power level, larger feedback gain is necessary to help suppress the environmental noise of the timing link. Compared with Fig. 8(a) and (b), it can be seen that as the link operational power decreases, both the shot noise and the electronic noise from the PI controller are elevated, while the electronic noise of BLOTD increases the most dramatically and becomes the major contributor to the increase of IDTJ. Nevertheless, the total out-of-loop timing jitter is still dominated by J_E and J_I.

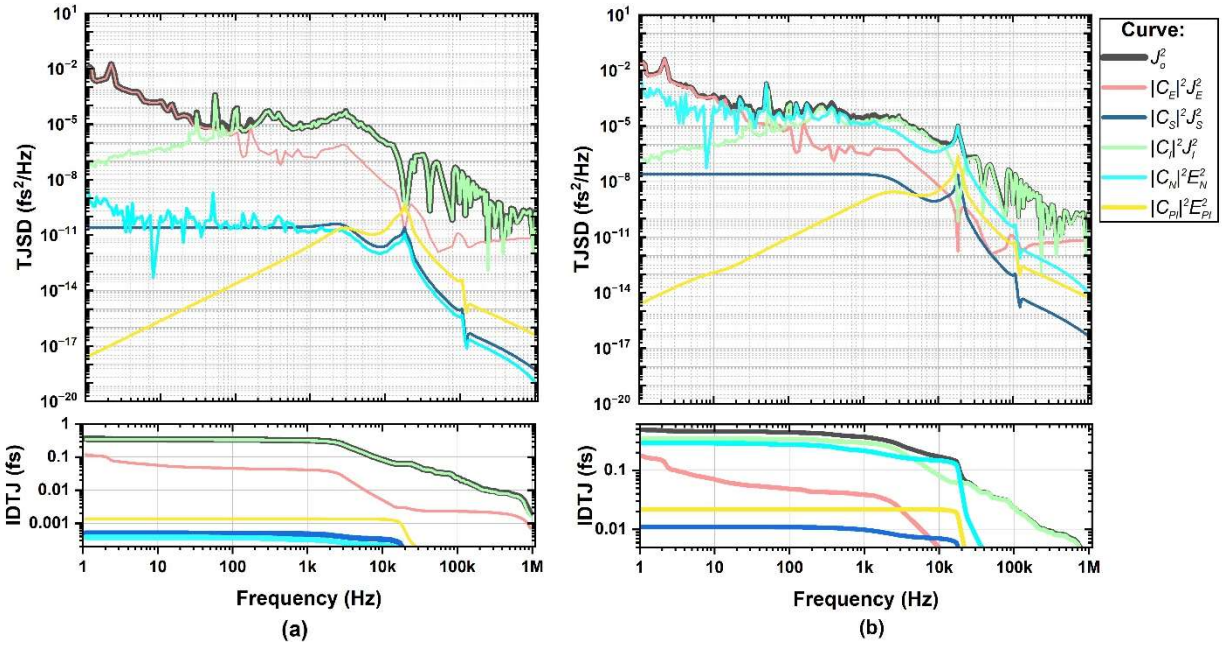

Fig. 8. Out-of-loop jitter simulation results of individual jitter contributions with the optical power of (a) 1mW and (b) 1μW at each PD of the in-loop BLOTD. The timing link length is 10.4 km. The legend on the right shows the color code of the jitter spectral densities. Integrated jitter in this graph is shown on a logarithmic scale.

Furthermore, timing link stabilization with different fiber lengths are also simulated. Keeping the in-loop PD power as 1 μW, an integrated timing jitter of 0.79 fs can still be achieved for 20-km link stabilization (Fig. 9(a)). While if the link length is reduced to 5.2 km, an unprecedented low optical power of 240 nW at each in-loop PD is sufficient to provide sub-fs link stabilization precision (with 0.93 fs integrated jitter, as shown in Fig. 9(b)). Leveraging the advantages of

https://doi.org/10.1017/hpl.2025.30 Published online by Cambridge University Press

BLOTD, we theoretically demonstrated the capability to extend the link length to nearly five times that of previous works using BOC, and the required operational power is also reduced by more than 3 orders of magnitude. This breakthrough overcomes the current power-imposed limitations on transmission distance and the number of synchronization terminals, holding significant implications for the expansion and construction of various large-scale laser facilities.

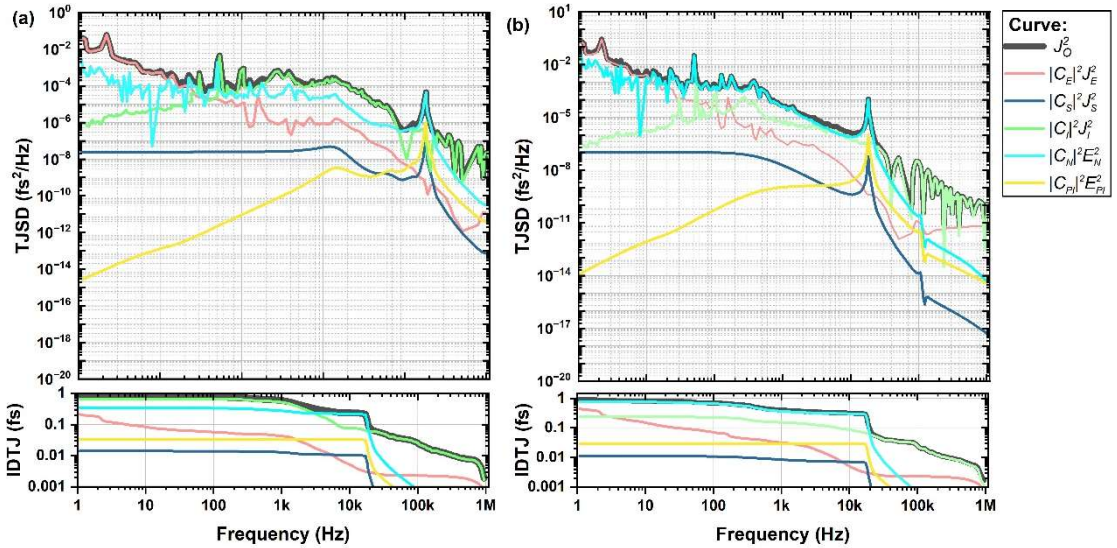

Fig. 9. Out-of-loop jitter simulation results of individual jitter contributions at the in-loop PD power of (a) 1 μW with transmission length of 20 km; (b) 240 nW with transmission length of 5.2 km.

VI Conclusions

In summary, we have experimentally demonstrated an attosecond-precision balanced linear-optics-based timing detector. With 1-mW power per pulse train per photodetector, a shot-noise-limited timing detection floor of 1×10^{-10} fs^2/Hz is achieved. The balanced configuration effectively mitigates environmental and laser amplitude noise. The total integrated jitter from 1 Hz to 1 MHz is merely 26.57 attoseconds. As one of the applications, we have conducted the residual dispersion evaluation with such a powerful tool. Finally, we have presented a comprehensive jitter analysis for the timing link stabilization. At 1-mW and 1-μW optical power at each PD of the in-loop

https://doi.org/10.1017/hpl.2025.30 Published online by Cambridge University Press

BLOTD, the 10.4-km link is stabilized with a total integrated jitter of 0.359 fs and 0.48 fs, respectively. The system can still maintain sub-fs precision with lower optical power or longer link length. For instance, with 5.2-km link length, an integrated jitter of 0.93 fs can be achieved with only 240 nW power; while with 1-μW power, after 20-km link transmission, the residual timing jitter is only 0. 79 fs.

We believe that the timing link stabilization at ultra-low optical power levels will not only greatly expand the distance and number of terminals of the current synchronization systems, but also be beneficial in many other cutting-edge fields such as ultra-long-range laser radar and gravitational wave detection.

Appendix

A. Noise sources characterization

The inherent jitter J_I is obtained from our previous BOC characterization results of a commercial MLL [28]. The shot-noise-equivalent timing jitter J_S can be calculated by the Eq. (9) of [24]. The electronic noise E_N of the BLOTD (generated from the photodetector, the bandpass filter, the RF amplifiers, the ZSD, and the differential amplifier) is measured when there is no input light in the system and then converted to timing jitter (in units of s/√Hz) by multiplying with the timing sensitivity. **The environmental noise jitter J_E is divided into two parts: at low frequencies (<100 Hz), the noise is modeled by a combination of $1/f$ and $1/f^2$ noise, reflecting the typical properties of environmental noise; for frequencies >100 Hz, the measured data from Ref. [29] is utilized.** The electronic noise of the PI controller E_{PI} is evaluated utilizing a noise model predicated with the characteristics of the amplifier circuits presented in Fig. 10 (a), and can be estimated by Eq. (25) and (26) [29].

https://doi.org/10.1017/hpl.2025.30 Published online by Cambridge University Press

$$E_{PI}^2 = \frac{4Z_f^2 k_B T}{R_{in}} + 4k_B T R_f + \left(1 + \frac{Z_f}{R_{in}}\right)^2 V_n^2 \tag{25}$$

$$Z_f = \frac{1/R_f - j\omega C}{\left(1/R_f\right)^2 + \omega^2 C^2} \tag{26}$$

B. Transfer functions calculation

The transfer functions H_{BLD}, H_{DA}, H_{PI} and H_{FS} in Fig. 6 can be obtained by the following equations:

$$H_{BLD} = k_{BLD} \tag{27}$$

$$H_{PI} = k_{PI}\left(\frac{s + 2\pi f_{PI}}{s}\right) \tag{28}$$

$$H_{DA} = \left(1 + \frac{s}{2\pi f_{BW}}\right)^{-1} \tag{29}$$

$$H_{FS} = H_{PZT} H_F \tag{30}$$

where k_{BLD} is the sensitivity of the BLOTD (in units of mV/fs), k_{PI} is the PI gain, f_{PI} is the PI corner frequency, f_{BW} is the 3-dB bandwidth of the differential amplifier. The transfer function H_{FS} is the product of two parts: the PZT response function H_{PZT} fitted from manufacturer data and the filter function H_F by the equivalent driven circuits (shown in Fig. 10(b)) [30].

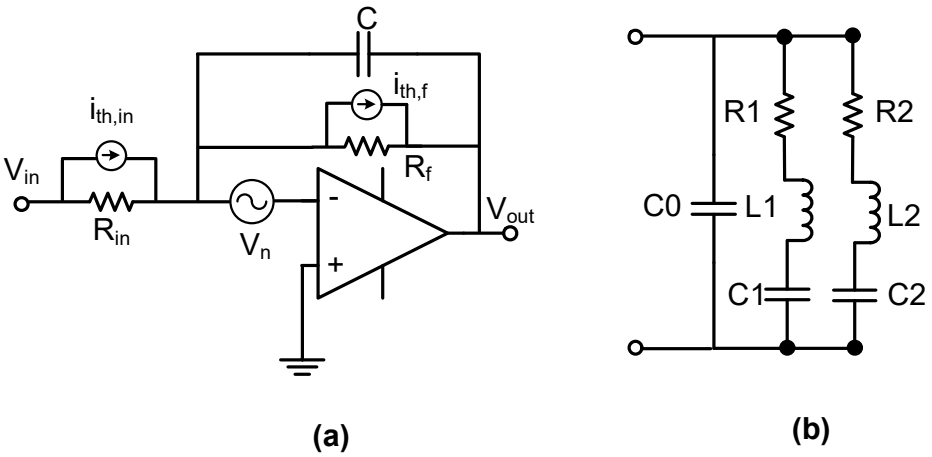

Fig 10. (a)Noise model of the PI controller. V_{in} and V_{out}: input and output voltage; V_n: input voltage noise of the PI controller; R_{in} and $i_{th,in}$: input impedance and its thermal noise current; R_f and $i_{th,f}$: feedback gain resistance and its thermal noise current; C: integrating capacitance. (b)Equivalent circuit of the fiber stretcher.

C. Typical parameters of the link stabilization used for simulation

https://doi.org/10.1017/hpl.2025.30 Published online by Cambridge University Press

Table 1

Parameter:	Value:	Unit:
k_{BLD}	43.57 (with 1 mW input power)	mV/fs
f_{rep}	216.667	MHz
f_{BW}	1	MHz
R_{in}	1	MΩ
R_f	$k_{PI} \times R_{in}$	MΩ
C	10	nF
V_n	10^{-9}	V/√Hz
C_0	33	nF
C_1	5	nF
C_2	7	nF
R_1	26	Ω
R_2	3.2	Ω
L_1	15	mH
L_2	0.3	mH
T	300	K

https://doi.org/10.1017/hpl.2025.30 Published online by Cambridge University Press

Acknowledgement

This work was supported by the National Key R&D Program of China (Grant No. 2021YFC2201902) and National Natural Science Foundation of China (Grant No. 61975149).

References

[1] M. Xin, K. Şafak, and F. X. Kärtner, "Ultra-precise timing and synchronization for large-scale scientific instruments," *Optica*, vol. 5, no. 12, p. 1564, Dec. 2018, doi: 10.1364/OPTICA.5.001564.

[2] Z. Lin, X. Deng, D. Fan, S. Wang, S. Chen, J. Zhu, L. Qian, X. Shen, F. Xu, J. Zhu, W. Ma, X. Xie, Y. Zheng, W. Zhang, Q. Chen, M. Ling, H. Huang, and J. Zhang, "SG-II laser elementary research and precision SG-II program," *Fusion Engineering and Design*, vol. 44, no. 1–4, pp. 61–66, Feb. 1999, doi: 10.1016/S0920-3796(98)00308-1.

[3] S.-W. Bahk, P. Rousseau, T. A. Planchon, V. Chvykov, G. Kalintchenko, A. Maksimchuk, G. A. Mourou, and V. Yanovsky, "Generation and characterization of the highest laser intensities (10^{22} W/cm^2)," *Opt. Lett.*, vol. 29, no. 24, p. 2837, Dec. 2004, doi: 10.1364/OL.29.002837.

[4] V. Yanovsky, V. Chvykov, G. Kalinchenko, P. Rousseau, T. Planchon, T. Matsuoka, A. Maksimchuk, J. Nees, G. Cheriaux, G. Mourou, and K. Krushelnick, "Ultra-high intensity-300-TW laser at 0.1 Hz repetition rate," *Opt. Express*, vol. 16, no. 3, p. 2109, 2008, doi: 10.1364/OE.16.002109.

[5] Z. Zhang, F. Wu, J. Hu, X. Yang, J. Gui, P. Ji, X. Liu, C. Wang, Y. Liu, X. Lu, Y. Xu, Y. Leng, R. Li, and Z. Xu, "The laser beamline in SULF facility," *High Pow Laser Sci Eng*, vol. 8, p. e4, 2020, doi: 10.1017/hpl.2020.3.

[6] A. S. Pirozhkov, Y. Fukuda, M. Nishiuchi, H. Kiriyama, A. Sagisaka, K. Ogura, M. Mori, M. Kishimoto, H. Sakaki, N. P. Dover, K. Kondo, N. Nakanii, K. Huang, M. Kanasaki, K. Kondo, and M. Kando, "Approaching the diffraction-limited, bandwidth-limited Petawatt," *Opt. Express*, vol. 25, no. 17, p. 20486, Aug. 2017, doi: 10.1364/OE.25.020486.

[7] G. Tiwari, E. Gaul, M. Martinez, G. Dyer, J. Gordon, M. Spinks, T. Toncian, B. Bowers, X. Jiao, R. Kupfer, L. Lisi, E. McCary, R. Roycroft, A. Yandow, G. D. Glenn, M. Donovan, T. Ditmire, and B. M. Hegelich, "Beam distortion effects upon focusing an ultrashort petawatt laser pulse to greater than 10^{22} W/cm^2," *Opt. Lett.*, vol. 44, no. 11, p. 2764, Jun. 2019, doi: 10.1364/OL.44.002764.

[8] K. L. Baker, D. Homoelle, E. Utterback, and S. M. Jones, "Phasing rectangular apertures," *Opt. Express*, vol. 17, no. 22, p. 19551, Oct. 2009, doi: 10.1364/OE.17.019551.

[9] J.-P. Chambaret, O. Chekhlov, G. Chériaux, J. Collier, R. Dabu, P. Dombi, A. M. Dunne, K. Ertel, P. Georges, J. Hebling, J. Hein, C. Hernandez-Gomez, C. Hooker, S. Karsch, G. Korn, F. Krausz, C. L. Blanc, Z. Major, F. Mathieu, T. Metzger, G. Mourou, P. Nickles, K. Osvay, B. Rus, W. Sandner, G. Szabó, D. Ursescu, and K. Varjú, "Extreme Light Infrastructure: architecture and major challenges," Proc. SPIE 7721, Solid State Lasers and Amplifiers IV, and High-Power Lasers, 77211D, May 2010, doi:10.1117/12.854687.

[10] A. V. Bashinov, A. A. Gonoskov, A. V. Kim, G. Mourou, and A. M. Sergeev, "New horizons for extreme light physics with mega-science project XCELS," *Eur. Phys. J. Spec. Top.*, vol. 223, no. 6, pp. 1105–1112, May 2014, doi: 10.1140/epjst/e2014-02161-7.

[11] J. P. Zou, C. Le Blanc, D. N. Papadopoulos, G. Chériaux, P. Georges, G. Mennerat, F. Druon, L. Lecherbourg, A. Pellegrina, P. Ramirez, F. Giambruno, A. Fréneaux, F. Leconte, D. Badarau, J. M. Boudenne, D. Fournet, T. Valloton, J. L. Paillard, J. L. Veray, M. Pina, P. Monot, J. P. Chambaret, P. Martin, F. Mathieu, P. Audebert, and F. Amiranoff, "Design and current progress of the Apollon 10 PW project," *High Pow Laser Sci Eng*, vol. 3, p. e2, 2015, doi: 10.1017/hpl.2014.41.

[12] S. Gales, K. A. Tanaka, D. L. Balabanski, F. Negoita, D. Stutman, O. Tesileanu, C. A. Ur, D. Ursescu, I. Andrei, S. Ataman, M. O. Cernaianu, L. D'Alessi, I. Dancus, B. Diaconescu, N. Djourelov, D. Filipescu, P. Ghenuche, D. G. Ghita, C. Matei, K. Seto, M. Zeng, and N. V. Zamfir, "The extreme light infrastructure—nuclear physics (ELI-NP) facility: new horizons in physics with 10 PW ultra-intense lasers and 20 MeV brilliant gamma beams," *Rep. Prog. Phys.*, vol. 81, no. 9, p. 094301, Sep. 2018, doi: 10.1088/1361-6633/aacfe8.

[13] J. Bromage, S.-W. Bahk, I. A. Begishev, C. Dorrer, M. J. Guardalben, B. N. Hoffman, J. B. Oliver, R. G. Roides, E. M. Schiesser, M. J. Shoup Iii, M. Spilatro, B. Webb, D. Weiner, and J. D. Zuegel, "Technology development for ultraintense all-OPCPA systems," *High Pow Laser Sci Eng*, vol. 7, p. e4, 2019, doi: 10.1017/hpl.2018.64.

[14] X. Wang, X. Liu, X. Lu, J. Chen, Y. Long, W. Li, H. Chen, X. Chen, P. Bai, Y. Li, Y. Peng, Y. Liu, F. Wu, C. Wang, Z. Li, Y. Xu, X. Liang, Y. Leng, and R. Li, "13.4 fs, 0.1 Hz OPCPA Front End for the 100 PW-Class Laser Facility," *Ultrafast Science*, Jun, 2022, doi:10.34133/2022/9894358.

[15] M. Altarelli, Ed., XFEL, the European X-ray free-electron laser: technical design report. Hamburg: DESY XFEL Project Group, 2006.

[16] E. Allaria, R. Appio, L. Badano, W. A. Barletta, S. Bassanese, S. G. Biedron, A. Borga, E. Busetto, M. Zangrando, *et al.*, "Highly coherent and stable pulses from the FERMI seeded free-electron laser in the extreme ultraviolet," *Nature Photon*, vol. 6, no. 10, pp. 699–704, Oct. 2012, doi: 10.1038/nphoton.2012.233.

[17] P. Emma, R. Akre, J. Arthur, R. Bionta, C. Bostedt, J. Bozek, A. Brachmann, P. Bucksbaum, R. Coffee, F.-J. Decker, Y. Ding, D. Dowell, S. Edstrom, A. Fisher, J. Frisch, S. Gilevich, J. Hastings, G. Hays, Ph. Hering, Z. Huang, R. Iverson, H. Loos, M. Messerschmidt, A. Miahnahri, S. Moeller, H.-D. Nuhn, G. Pile, D. Ratner, J. Rzepiela, D. Schultz, T. Smith, P. Stefan, H. Tompkins, J. Turner, J. Welch, W. White, J. Wu, G. Yocky, and J. Galayda, "First lasing and operation of an ångstrom-wavelength free-electron laser," *Nature Photon*, vol. 4, no. 9, pp. 641–647, Sep. 2010, doi: 10.1038/nphoton.2010.176.

[18] J. Stohr, "Linac Coherent Light Source II (LCLS-II) Conceptual Design Report," SLAC-R-978, 1029479, Nov. 2011. doi: 10.2172/1029479.

[19] E. Prat and S. Reiche, "Simple Method to Generate Terawatt-Attosecond X-Ray Free-Electron-Laser Pulses," *Phys. Rev. Lett.*, vol. 114, no. 24, p. 244801, Jun. 2015, doi: 10.1103/PhysRevLett.114.244801.

[20] M. Xin, K. Şafak, M. Y. Peng, A. Kalaydzhyan, W.-T. Wang, O. D. Mücke, and F. X. Kärtner, "Attosecond precision multi-kilometer laser-microwave network," *Light Sci Appl*, vol. 6, no. 1, pp. e16187–e16187, Jul. 2016, doi: 10.1038/lsa.2016.187.

[21] H. A. Haus and A. Mecozzi, "Noise of mode-locked lasers," *IEEE J. Quantum Electron.*, vol. 29, no. 3, pp. 983–996, Mar. 1993, doi: 10.1109/3.206583.

https://doi.org/10.1017/hpl.2025.30 Published online by Cambridge University Press

[22] L. A. Jiang, S. T. Wong, M. E. Grein, E. P. Ippen, and H. A. Haus, "Measuring timing jitter with optical cross correlations," *IEEE Journal of Quantum Electronics*, vol. 38, no. 8, pp. 1047–1052, Aug. 2002, doi: 10.1109/JQE.2002.800993.

[23] T. R. Schibli, J. Kim, O. Kuzucu, J. T. Gopinath, S. N. Tandon, G. S. Petrich, L. A. Kolodziejski, J. G. Fujimoto, E. P. Ippen, and F. X. Kärtner, "Attosecond active synchronization of passively mode-locked lasers by balanced cross correlation," *Optics Letters,* vol. 28, no. 11, p. 947-9, Jun. 2003, doi: 110.1364/OL.28.000947.

[24] T. Wang, Q. Ren, K. Şafak, F. X. Kärtner, and M. Xin, "An attosecond-precision balanced linear timing detector," *Opt. Express*, vol. 29, no. 23, p. 38140-9, Nov 2023, doi: 10.1364/OE.442459.

[25] H. A. Haus, "Mode-locking of lasers," *IEEE Journal of Selected Topics in Quantum Electronics*, vol. 6, no. 6, pp. 1173–1185, Nov. 2000, doi: 10.1109/2944.902165.

[26] V. Giovannetti, S. Lloyd, and L. Maccone, "Quantum-enhanced positioning and clock synchronization," *Nature*, vol. 412, pp. 417–419, Jun, 2001, doi: 10.1038/35086525.

[27] J. P. Gordon and H. A. Haus, "Random walk of coherently amplified solitons in optical fiber transmission," *Optics Letters*, vol. 11, no. 10, pp. 665–667, 1986, doi: 10.1364/OL.11.000665.

[28] K. Şafak, M. Xin, P. T. Callahan, M. Y. Peng, and F. X. Kärtner, "All fiber-coupled, long-term stable timing distribution for free-electron lasers with few-femtosecond jitter," *Structural Dynamics*, vol. 2, no. 4, p. 041715, Jul. 2015, doi: 10.1063/1.4922747.

[29] K. Şafak, M. Xin, Q. Zhang, S.-H. Chia, O. D. Mücke, and F. X. Kärtner, "Jitter analysis of timing-distribution and remote-laser synchronization systems," *Opt. Express*, vol. 24, no. 19, p. 21752, Sep. 2016, doi: 10.1364/OE.24.021752.

[30] https://www.optiphase2.com/

https://doi.org/10.1017/hpl.2025.30 Published online by Cambridge University Press